



## Low-light image enhancement based on virtual exposure<sup>☆</sup>

Wencheng Wang <sup>a,\*</sup>, Dongliang Yan <sup>b</sup>, Xiaojin Wu <sup>a,\*\*</sup>, Weikai He <sup>b</sup>, Zhenxue Chen <sup>c</sup>, Xiaohui Yuan <sup>d</sup>, Lun Li <sup>a</sup>



<sup>a</sup> College of Machinery and Automation, Weifang University, Weifang, 261061, China

<sup>b</sup> ShanDong JiaoTong University, Jinan, 250062, China

<sup>c</sup> College of Control Science and Engineering, Shandong University, Jinan, 250061, China

<sup>d</sup> College of Engineering, University of North Texas, Denton, TX, 76207, USA

### ARTICLE INFO

#### Keywords:

Low-light image enhancement  
Virtual exposure  
Image fusion  
Gamma correction  
Camera response function

### ABSTRACT

Under poor illumination, the image information captured by a camera is partially lost, which seriously affects the visual perception of the human. Inspired by the idea that the fusion of multiexposure images can yield one high-quality image, an adaptive enhancement framework for a single low-light image is proposed based on the strategy of virtual exposure. In this framework, the exposure control parameters are adaptively generated through a statistical analysis of the low-light image, and a virtual exposure enhancer constructed by a quadratic function is applied to generate several image frames from a single input image. Then, on the basis of generating weight maps by three factors, i.e., contrast, saturation and saliency, the image sequences and weight images are transformed by a Laplacian pyramid and Gaussian pyramid, respectively, and multiscale fusion is implemented layer by layer. Finally, the enhanced result is obtained by pyramid reconstruction rule. Compared with the experimental results of several state-of-the-art methods on five datasets, the proposed method shows its superiority on several image quality evaluation metrics. This method requires neither image calibration nor camera response function estimation and has a more flexible application range. It can weaken the possibility of overenhancement, effectively avoid the appearance of a halo in the enhancement results, and adaptively improve the visual information fidelity.

### 1. Introduction

DIGITAL image processing systems are widely used in video surveillance, intelligent transportation, remote sensing, and play an increasingly important role in every aspect of human's lives. However, under poor lighting conditions such as indoors, nighttime, and overcast weather, the light reflected from the surface of an object is weak, causing color distortion and noise and thus poor quality of the acquired image [1–3]. In the  $24 \times 7$  scenarios, such as video surveillance, intelligent transportation, and autonomous driving, low-light environments not only influence the visual perception of the human eye but also affect the recognition accuracy of machine systems, even causing the failure of these systems [4]. Traditional schemes using supplementary infrared lighting can yield clear images in a completely light-free environment but can generate only monochrome (grayscale) images

that lack color information and are affected by noise. Therefore, in various fields, the details of low-light images acquired under poor lighting conditions must be enhanced, and the color information of scene images require maximal restoration [5]. Fig. 1 shows some images captured in poor lighting environments, i.e., nighttime, overcast weather, uneven illumination, and backlighting. It can be seen that the partial overexposure or underexposure result in the loss of edge information and texture details.

Therefore, it is valuable to make images more consistent with human subjective visual perception and to improve the computer vision capability through image enhancement. Many effective algorithms have been proposed; however, these methods often have many parameters and tend to overenhance some local areas with uneven illumination; moreover, they struggle to strike a balance between processing speed and effect. Against this background, we developed a method for enhancing single low-light images by using image fusion strategy. This

<sup>☆</sup> This work was supported by Natural Foundation of Shandong Province (No. ZR2023MF047), Science and Technology Plan for Youth Innovation of Shandong's Universities (No. 2019KJN012), Science and Technology Development Plan of Weifang City (No. 2021GX006), China University Industry-University-Research Innovation Foundation (No. 2021ZYA11003, 2021ITA05032), Science and Technology SMEs Innovation Capacity Improvement Project of Shandong (2022TSGC1248) and National Natural Science Foundation of China (Grant No. 61403283).

\* Corresponding author.

\*\* Corresponding author.

E-mail addresses: [wwcwf@126.com](mailto:wwcwf@126.com) (W. Wang), [dongliang9845@163.com](mailto:dongliang9845@163.com) (D. Yan), [wfuwxj@163.com](mailto:wfuwxj@163.com) (X. Wu), [214035@sdtu.edu.cn](mailto:214035@sdtu.edu.cn) (W. He), [chenzhenxue@sdu.edu.cn](mailto:chenzhenxue@sdu.edu.cn) (Z. Chen), [xiaohui.yuan@unt.edu](mailto:xiaohui.yuan@unt.edu), [zhinanqiao@my.unt.edu](mailto:zhinanqiao@my.unt.edu) (X. Yuan), [l1408907652@163.com](mailto:l1408907652@163.com) (L. Li).

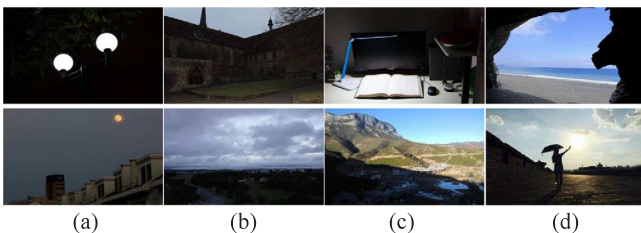


**Fig. 1.** Various conditions that negatively affect image quality, such as (a) nighttime; (b) overcast; (c) uneven illumination; and (d) backlighting.

method automatically simulates the exposure of each image, then uses the contrast, saturation, and saliency of the image as the criterion to calculate the perceived quality, and, under the guidance of the above quality metrics, chooses useful pixels from the sequence to fuse into a final result. Compared to previous work, our method offers the following contributions:

- It is a simple and effective image enhancer based on the strategies of virtual exposure and image fusion. This method can reveal more information in extremely dark areas while preserving the details of whole image;
- In this framework, exposure control parameters are adaptively generated through the statistical analysis on a single input low-light image, which requires neither image calibration nor camera response function;
- A virtual exposure enhancer constructed by means of a quadratic function is applied to generate several image frames from only one low-light image;
- This method does not need a large number of data sets for training, and has a flexible application range; it and can produce the satisfied results with less computational complexity.

The rest of this paper is organized as follows. The second section briefly introduces previous work about low-light image enhancement. In the third section, the proposed algorithm and the strategy of combining the virtual exposure technique with the multiscale image fusion technique are described in detail. In Section 4, the experimental results are analyzed, and the conclusion is presented in Section 5.

## 2. Related works

In this section, the related work on low-light image enhancement is introduced. The current methods can be divided into four categories: histogram-based methods, retinex-based methods, dehazing-based methods and learning-based methods.

Histogram-based methods can enhance images by regulating the gray-level distribution [6]. For example, Kim et al. [7] proposed an adaptive histogram equalization method with block iteration. Reza et al. [8] proposed the contrast-limited adaptive histogram equalization (CLAHE) algorithm, which can avoid image overenhancement. Later, CLAHE was improved by integrating a learning-based hyperparameter selection method to enhance the image contrast while preserving the naturalness of the image content [9]. Celik et al. [10] used a two-dimensional histogram and context information model of input image to perform nonlinear mapping and proposed a variable-contrast algorithm to realize low-light image enhancement. Parihar et al. [11] proposed an entropy-based dynamic subhistogram equalization method, in which a new dynamic range is assigned to each subhistogram in accordance with the entropy and gray levels. Gu et al. [12] applied a quality evaluation model to optimize the histogram parameters in order to effectively address the problem of overenhancement. Liu et al. proposed a stratified parametric-oriented histogram equalization method, which can effectively achieve a regional enhancement effect without visual artifacts [13]. Zarie et al. proposed a robust enhancement method,

i.e., triple clipped dynamic histogram equalization based on the standard deviation (TCDHE-SD), which separates the image histogram into three parts [14]. Histogram equalization algorithms can effectively improve the contrast and detail information of low-light images but also can easily cause color loss and image distortion. Therefore, these algorithms are often used in combination with other methods.

Retinex-based methods operate on the basis of a color constancy theory known as retinal-cortex, or retinex theory. Initially, the single-scale retinex algorithm was proposed for image enhancement. It was then further developed into classic algorithms such as the multiscale retinex (MSR) algorithm, the MSR with color restoration (MSRCR) algorithm [15,16] and the MSR with chromaticity preservation (MSRCP) algorithm [17]. In addition, Xu et al. [18] present a novel structure and texture aware retinex (STAR) model for illumination and reflectance decomposition of a single image to improve the performance of low-light image enhancement. Wang et al. [19] proposed a naturalness-preserving enhancement method by combining a bright-pass filter with neighborhood information, which can not only improve the contrast of an image but also weaken local overenhancement. Fu et al. realized image enhancement by developing a weighted variational model for simultaneous reflection and illumination estimation (SRIE) [20]. After separating the reflection and brightness components based on retinex theory, some scholars have incorporated filter factors to avoid noise amplification [21,22] or have adjusted the degrees of enhancement for different brightness values to weaken color distortion [23]. Gu et al. proposed a retinex-based fractional-order variational model for severely low-light images, which can yield an appropriate estimate of reflectance and preserve small-magnitude details in the enhancement results [24]. Ren et al. introduced a robust low-light enhancement approach based on the low-rank regularized retinex model (LR3M) to suppress noise in the reflectance map and achieved satisfactory enhancement and denoising performance [25]. Retinex-based algorithms have a clear physical meaning and are easy to implement; however, these algorithms have a high computational complexity and can easily produce halo artifacts in the restored images.

The dehazing-based approach was first developed based on the observation that the characteristics of an inverted low-light image are similar to those of a hazy image [26]. Later, the related algorithms were optimized. For example, Yu et al. [27] adopted a convolutional neural network (CNN) to solve for the transmittance and used the local atmospheric light value as the global atmospheric light value. The resulting enhanced images show good performance in terms of the average gradient and information entropy. Zhang et al. [28] proposed a real-time enhancement method that combines dehazing technology and filtering technology, in which a dark channel prior (DCP) is used for parameter estimation and a bilateral filter is used for noise reduction. Later, Hu et al. [29] proposed a fast enhancement algorithm that combines retinex theory and DCP for processing low-light video sequences. As an alternative form of a DCP, a bright channel prior (BCP) is usually used in combination with a retinex enhancement algorithm [30]. Tao et al. [31] combined a BCP with CNNs to train an image enhancement model, while Park et al. used an unsupervised loss function and a simple encoder-decoder architecture to achieve satisfactory experimental results [32]. The dehazing-based methods offer good performance with low computational complexity. However, their physical interpretability is somewhat lacking, and they are still susceptible to overenhancement in some areas.

Learning-based methods for image enhancement have seen rapid development in recent years. For example, Lore et al. [33] used a stacked sparse denoising autoencoder in an image enhancement framework and trained a self-encoder on the characteristics of various low-light images to achieve adaptive brightness adjustment and denoising. Shen et al. [34] analyzed the performance of the MSR algorithm from the CNN perspective and proposed a low-light image enhancement method using an MSR network with a CNN architecture. Tao et al. proposed a low-light CNN (LLCNN) [35], in which multilevel characteristic images

are used to form enhanced images by learning the features of low-light images with different kernels. Wei et al. assumed that images could be decomposed into reflectance and illumination components and proposed a deep network called RetinexNet [36] after collecting a low-light (LoL) dataset consisting of low-light/normal-light image pairs. Lv et al. proposed a multibranch low-light enhancement network (MBLLEN) consisting of a feature extraction module, an enhancement module and a fusion module (FM) [37], which outputs images via feature fusion. Gharbi et al. designed a deep bilateral learning framework to realize real-time image enhancement [38]. Wang et al. [39] designed a global illumination-aware and detail-preserving network (GLADNet) based on a global prior and the original images and used a convolutional network to reconstruct the image details. Li et al. designed a network called LightenNet [40] that takes a weakly illuminated image as its input and outputs a corresponding illumination map, which is subsequently used to generate an enhanced image based on the retinex model. Zhang et al. built a simple yet effective network called the Kindling the Darkness network (KinD) [41], which is composed of a layer decomposition net, a reflectance restoration net and an illumination adjustment net, and trained it on pairs of images captured under different exposure conditions. Meng et al. [42] proposed a generative adversarial network (GAN)-based framework for nighttime image enhancement, which takes advantage of the powerful ability of GANs to generate images from real data distributions; their results demonstrated its effectiveness. Methods of this kind perform well, but their computational models often require too much time or too many resources for training.

### 3. Virtual exposure for image enhancement

The details of the different areas in each image are related to the degree of exposure of the acquisition device. When images are captured with low exposure, the details of well-lit areas are visible, but those of dark areas are largely lost; conversely, when images are captured with high exposure, the details of dark areas are visible, but those of well-lit areas are lost [43,44]. To solve this problem, the multiexposure fusion technique was developed, which can fuse images with different exposure levels to generate a new image with rich details. This technique has been widely used in the generation of high-dynamic-range images. However, since this method requires multiframe images of the same scene, its applicability is limited. More recently, methods based on the fusion of different images derived from a single low-light image have been proposed. For example, Fu et al. [45] carried out image fusion after applying the tangent transform and the CLAHE operation to the intensity component in order to enhance the brightness of low-light images, while Ancuti et al. [46] realized underwater image enhancement by fusing white-balanced and filtered images. However, these algorithms neither simulate the physical process of image exposure nor enhance the color; hence, they are not suitable for uneven-light image enhancement.

Inspired by the above ideas, we have designed a virtual exposure enhancer that converting single image into a multiframe sequence of images based on the analysis of various low-light images, and combining this process with the multiscale image fusion technique to achieve adaptive low-light image enhancement. The whole framework of the algorithm is shown in Fig. 2. When the input is a single low-light image, virtual exposure images are obtained by processing the original image through the virtual exposure enhancer, which is constructed by means of a brightness correction function. A weight map for each image in the sequence is then generated based on three information factors: contrast, saturation, and saliency. The generated images are subjected to Laplacian pyramid decomposition, while Gaussian pyramid decomposition is applied to the corresponding weight maps. The virtual exposure images with the same resolution are then multiplied by the weight maps at the corresponding scale. Finally, the image information is added together, and the enhanced image is obtained through pyramid reconstruction once fusion is completed.

#### 3.1. Virtual exposure enhancer

The multiexposure fusion technique allows us to use a sequence of images with different exposure levels to synthesize the clear information of that image sequence into a new image; it can effectively improve the rate of utilization of image information to facilitate either human visual observation or computer processing. Its working principle can be expressed as follows:

$$I_e = F \{ I_i \}, \quad (1)$$

where  $I_i$  is the  $i$ th image of the image sequence to be fused,  $I_e$  is the fused image, and  $F\{\cdot\}$  is the fusion function.

When a single low-light image is considered, to generate other image sequences for fusion, the simplest processing method is to directly enhance the low-light image by using a tone mapping operator, in which each gray-level enhancement is equivalent to performing grayscale expansion and brightness enhancement on a certain region in a targeted manner so that  $I_i \leftarrow I_0$ . Suppose that the original image is represented as  $I_0$ , and  $f_i(\cdot)$  is the image grayscale conversion function. Then, the image after processing is completed is as follows:

$$I_i = f_i(I_0), \quad (2)$$

In Eq. (2),  $f_i$  must meet the monotonicity and boundedness requirements:

$$\mathbb{F} := \{f | f(0) = 0, f(1) = 1, x \geq y \Leftrightarrow f(x) \geq f(y)\}, \quad (3)$$

Since the brightness conversion result is not derived from the true exposure, it is referred to as a virtual exposure enhancer. For a virtual exposure enhancer to obtain different brightness conversion functions  $f_i$ , a control parameter  $k$  must be set up so that different conversion functions are obtained to achieve different exposure levels:

$$f_i = f(k_i), \quad (4)$$

Combining Eq. (4) with Eq. (2) yields

$$I_i = f(I_0, k_i), \quad (5)$$

Suppose that the parameter of image conversion is nonlinearly correlated with the overall brightness of the image scene. Then, inspired from the idea from Zero-DCE [4], the input-output relation of the virtual exposure enhancer established based on the image luminance control parameter can be expressed as a quadratic function:

$$f : \{y = x + k \times x(1 - x)\}, \quad (6)$$

In Eq. (6), the parameters of  $x$  and  $y$  represent the input and output, respectively, and  $k$  is the control coefficient. The function is differentiable in a certain range, and the slope decreases with the increasing input.

The low-light image is designated  $I_0$ , and the grayscale range is  $[0, 1]$ . Then, the pixel value of the  $i$ th virtual image  $I_i$  can be expressed as

$$I_i = \begin{cases} I_0 + k_i \times I_0(1 - I_0), & \text{if } I_0 + k_i \times I_0(1 - I_0) < 1 \\ 1, & \text{otherwise} \end{cases}, \quad (7)$$

where  $k_i$  (from  $k_1, k_2, k_3 \dots, k_N$ ) is the control coefficient of the  $i$ th exposure level. Although the gamma correction can also realize nonlinear enhancement of the image, its enhanced value cannot break through the limit of the output value of 1; thus, the process of strong exposure is difficult to simulate. In addition, the computational complexity gamma transform is far greater than quadratic function. After all the  $k_i$  values are input one by one into the virtual exposure enhancer,  $N$  virtual exposure images can be obtained. Fig. 3 shows a curve whose output is a function of the variable  $k$ . Clearly, as  $k$  increases, the slope of the curve also increases, as does the image brightness enhancement, indicating that the brightness of the generated image completely depends on the parameter of the virtual exposure enhancer and that by setting an appropriate  $k$  value, the desired image brightness can be obtained.

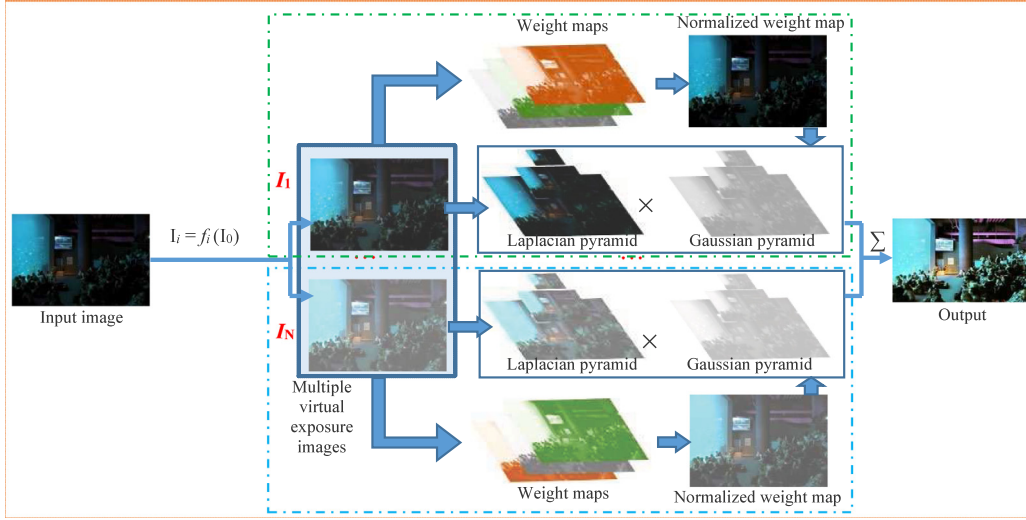


**Fig. 2.** Framework of the proposed algorithm. In this framework, single low-light image is converted into a multiframe sequence of images, and multiscale image fusion technique is adopted to achieve adaptive low-light image enhancement.

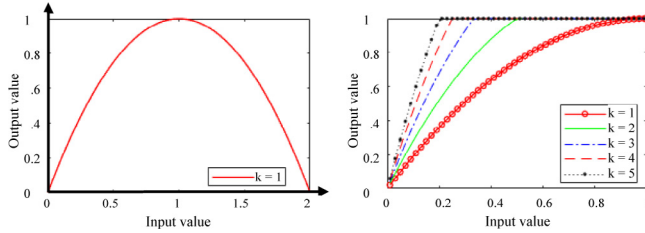


**Fig. 3.** Image conversion function curve. (The left curve is from Eq. (6) when \$k = 1\$, and the right is from Eq. (7) with the changes of \$k\$.)

To improve the adaptability of the algorithm, the average value of the virtual exposure image is used as the expected maximum to calculate \$k\$. Suppose that the average gray value of a virtual exposure image is \$\mu\_k\$ and that the expected value is \$\xi\$; then, the value of \$k\$ that allows \$\mu\_k\$ to maximally approximate \$\xi\$ is used as the control parameter. In addition, since the content and degree of exposure of the low-light images are different, to restrict the enhancement of virtual exposure, we constrain the estimated \$\hat{k}\$ empirically and set the maximum and minimum thresholds (\$k\_L \leq \hat{k} \leq k\_H\$). Therefore, the estimated \$\hat{k}\$ can be expressed as follows:

$$\hat{k} = \arg \min_k |\mu_k - \xi| (k_L \leq \hat{k} \leq k_H), \quad (8)$$

In practice, the expected value \$\xi\$ is set to 0.5 (the range of image gray values is [0, 1]), \$k\_H = 12\$ and \$k\_L = 6\$.

Using Eq. (8), the value of \$k\$ that allows the average image gray value to be \$\xi\$ after the enhancement is the maximum exposure, and after adjustment of the virtual exposure enhancer \$k\_i\$, \$N\$ images are obtained. The calculation formula is as follows:

$$k_i = (i \times k)/N, \quad (9)$$

In this work, the number of images was set to 5, i.e., a virtual exposure image sequence of five images with different exposure values was obtained. Fig. 4 shows the four virtual exposure images obtained through the extension using the above method and their corresponding histograms and pseudocolor images. It can be seen that the virtual exposure processing of low-light images through the function is equivalent to the extension and luminance stretch on a region in a targeted manner; thus, the underexposed image can well present the well-lit areas of the actual scene, while the overexposed image can well present the poorly lit areas of the actual scene. In addition, the original low-light images under different circumstances reveal that although the

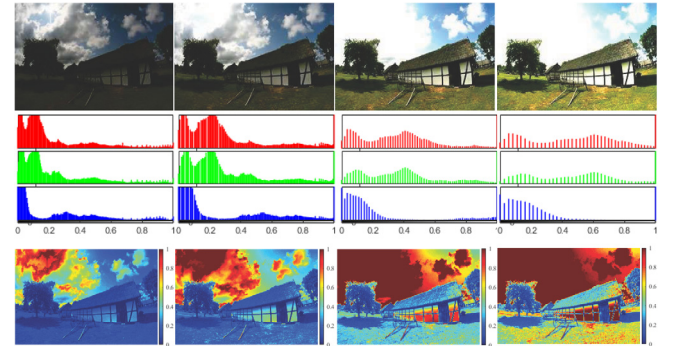


**Fig. 4.** Low-light image and its virtual exposure image sequence (the first row presents the virtual exposure images, the second row contains the histograms, and the third row shows the false-color luminance images).

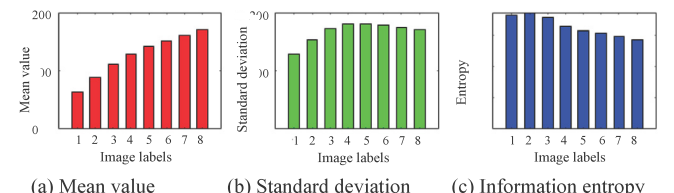


**Fig. 5.** Changes to the image statistical indicators with eight virtual exposure levels. (a)–(c) are used the indicators of mean value, standard deviation and information entropy, respectively.

information in the underexposed areas is partially hidden in the dark, well-exposed areas still have a good visual outcome and do not require the enhancement operation. Accordingly, to better utilize these pieces of information in the original image, the original low-light image needs to be included in the image sequence to be fused; thus, the image after enhancement appears more natural. The changes to the mean, standard deviation, and information entropy from before to after the enhancement of eight virtual exposures are shown in Fig. 5.

### 3.2. Weight maps

The simulated exposure image sequences are from the same scene, with highly related target contents but different focuses. Images with

proper exposure can show rich texture details and color information, while the overexposed and underexposed areas hardly convey any information; therefore, the choice of the weights is very important. To enable the fused image to be in line with the characteristics of the human visual system, among the  $N$  virtual exposure images, the smooth regions or unsaturated regions caused by overexposure or underexposure should be given a lower weight, while those with proper exposure and rich details should be given a higher weight. Against this background, three metrics, i.e., contrast, saturation, and visual saliency, are introduced in this study to fuse and restore image information.

(1) Contrast represents the degree of image detail: the higher the contrast is, the better the image detail presentation, and the easier the human eye can distinguish things in it. In this work, the absolute value after Laplacian filtering is used as the contrast factor, and the weight coefficient is obtained by calculating the changes at the image edges. Specifically, the image is first converted to a grayscale image, the pixel values are normalized to the  $[0, 1]$  interval, and the Laplacian filter is applied to the image, with the following expression and filter template:

$$C_{ij,k} = h * I, \quad (10)$$

$$h = \begin{vmatrix} 0 & 1 & 0 \\ 1 & -4 & 1 \\ 0 & 1 & 0 \end{vmatrix}, \quad (11)$$

In Eq. (10),  $C$  is the contrast,  $I$  is the image whose contrast is to be calculated, and  $h$  is the Laplacian filter.

The contrast calculated through this coefficient is mainly used to distinguish the gaps between one pixel and its neighbors; hence, the absolute value of the pixel at this position is taken as the final contrast parameter.

(2) Saturation is an important indicator that reflects the vividness and colorfulness of an image; the higher the saturation is, the more vivid the image. Saturation can quantify the red (R), green (G), and blue (B) channels of each pixel in an image and is obtained by calculating the standard deviations of the three chrominance channels. Specifically, the R, G, and B components of an image are extracted. Then, the averages of the R, G, and B components of each pixel in the image are calculated. Last, the standard deviation of the image color is calculated to determine the saturation coefficient  $S_{ij,k}$ :

$$S_{ij,k} = \sqrt{\frac{(I_R - \mu)^2 + (I_G - \mu)^2 + (I_B - \mu)^2}{3}}, \quad (12)$$

$$\mu = \frac{1}{3}(I_R + I_G + I_B), \quad (13)$$

In Eqs. (12) and (13),  $I_R$ ,  $I_G$ , and  $I_B$  are, respectively, the pixel values of the three chrominance channels (R, G, and B), and  $\mu$  is the mean of  $I_R$ ,  $I_G$ , and  $I_B$ .

(3) Saliency can accurately represent the importance of a pixel relative to its neighboring pixels [47]. Therefore, the construction of a fusion weight map based on saliency can effectively highlight the important parts of each fusion source without introducing noise. The construction of the saliency subweight graph can be expressed as:

$$A_{ij,k} = \|I_{u,k} - I_{g,k}\|, \quad (14)$$

In Eq. (14),  $A_{ij,k}$  is the saliency subweight map corresponding to the fusion source  $I_k$ ;  $I_{u,k}$  is the overall average of the fusion source in the three channels of the Lab color space; and  $I_{g,k}$  is obtained through Gaussian blurring of the fusion source in the Lab color space under a filter cutoff frequency of  $\omega_g = \pi/2.75$ . The saliency map is used to highlight the saliency areas in an image and enhance the contrast between the saliency area and its adjacent areas, thereby improving the global contrast of the image.

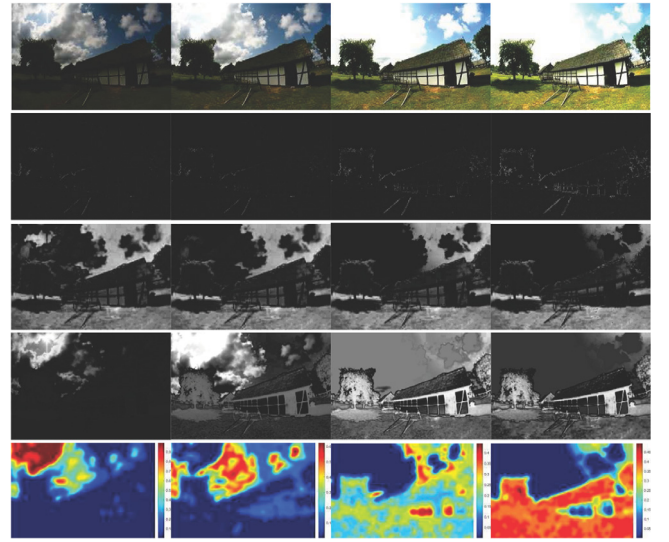


**Fig. 6.** Distribution of weight factors of a virtual multiexposure image. The first row presents the virtual exposure image sequence the second row corresponds to the contrast weight, the third row offers the saturation weight, the fourth row corresponds to the saliency weight, and the last row presents the normalized weight.

### 3.3. Multiresolution pyramid fusion

Traditional multiexposure fusion algorithms usually do not perform any image transformation on source images and do not take into account the correlations between pixels. Instead, they directly perform fusion processing on the corresponding pixels in the source image to yield a new image. Although simple and computationally light, these methods are unable to well represent the features in the source image, causing serious loss of texture details. Therefore, the existing spatial domain-based fusion rules must be improved and optimized to enhance the quality of image fusion without significantly affecting the computational complexity. The final weight is the product of the three weights, and the three weights simultaneously constrain the final weight. The formula is as follows:

$$W_{ij,k} = (C_{ij,k})^{\omega_c} \times (S_{ij,k})^{\omega_s} \times (A_{ij,k})^{\omega_a}, \quad (15)$$

where  $ij, k$  is the pixel  $(i, j)$  of the  $k$ th image;  $C_{ij,k}$ ,  $S_{ij,k}$ , and  $A_{ij,k}$  are, respectively, the contrast, saturation, and saliency of pixel  $(i, j)$  of the  $k$ th image; and  $\omega_c$ ,  $\omega_s$ , and  $\omega_a$  are used to control the impacts of the contrast factor  $C$ , the saturation factor  $S$ , and the saliency factor  $A$  on the weight map. For each fusion source, the weight map is equally important; thus, the algorithm sets  $\omega_c = \omega_s = \omega_a = 1$ , i.e., the three factors have the same impact on the generation of the new weight map.

**Fig. 6** shows the weight distribution of images with different exposure levels, in which the first row presents the virtual exposure image sequence  $I_k$ , the second row corresponds to the contrast weight  $C_k$ , the third row offers the saturation weight  $S_k$ , the fourth row corresponds to the saliency weight  $A_k$ , and the last row presents the normalized weight  $W_k$ . **Fig. 7** shows that the constructed saliency subweight map can effectively outline the essential part of the image, being able to effectively enhance unexposed regions of the low-light image while effectively retaining the properly exposed regions of the original image without introducing any artifacts.

To obtain consistent results, the weight of each exposure image is normalized to obtain the weight of pixel  $(i, j)$  of the  $k$ th image of the  $N$  multiexposure images:

$$\hat{W}_{ij,k} = \left[ \sum_{k=1}^N (W_{ij,k}) + \epsilon \right]^{-1} (W_{ij,k}), \quad (16)$$

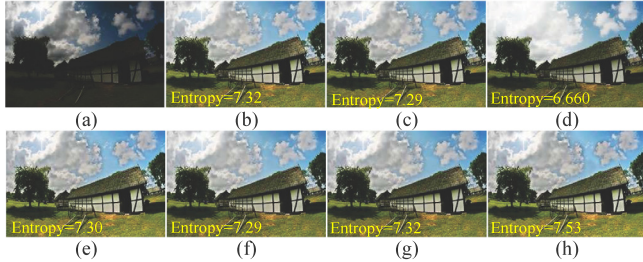


**Fig. 7.** Influence of different weight combinations. (b)–(d) are the fusion results using the contrast, saturation, and saliency weights, respectively; and (e)–(h) are the fusion results using the contrast + saturation, contrast + saliency, saturation + saliency weights, and contrast + saturation + saliency weights.

In Eq. (16), to avoid the situation where the denominator is zero,  $\epsilon$  is introduced. Here, we set  $\epsilon = 10^{-12}$ .

The final enhanced image is obtained by fusing the multiexposure images with the weight map, and the resulting image can be expressed as follows:

$$R_{ij} = \sum_{k=1}^N \hat{W}_{ij,k} \times I_{ij,k}, \quad (17)$$

where  $R_{ij}$  is the pixel value of the fused image at  $(i, j)$ ;  $I_{ij,k}$  is the pixel value of the corresponding position of the  $k$ th input image; and  $\hat{W}_{ij,k}$  is the normalized weight. This method is essentially a weighted average fusion method. If the fusion is performed directly, obvious gaps will appear due to sharp changes in the weight map.

Fig. 7 shows the results of direct fusion using different weighting factors, in which Fig. 7(a) is the source image; Fig. 7(b)–(d) are the fusion results obtained using the contrast, saturation, and saliency weights, respectively; and Fig. 7(e)–(h) are the fusion results obtained using the contrast + saturation weights, contrast + saliency weights, saturation + saliency weights, and contrast + saturation + saliency weights, respectively. On the basis of a human evaluation, the influences of different weight combinations in Fig. 7 do not show significant differences, except for (d). Therefore, the information entropy is provided to explain the influences. The results indicate that the overall image fusion effect is not good and that it is prone to cause a discrete halo effect in the final enhancement result. Although Gaussian smoothing or bilateral filtering can be used to eliminate the halo effect, either can introduce blurs at the edges.

To avoid the halo effect caused by sharp weight changes, the pyramid strategy is introduced into the algorithm to decompose the image and achieve image fusion in a multiresolution way. First, the multiexposure images are subjected to Laplacian pyramid decomposition and the weighted maps are subjected to Gaussian pyramid decomposition to generate images with different resolutions, in which  $G$  and  $L$ , respectively, represent the Gaussian pyramid operation and the Laplacian operation.

The  $l$ th layer of image  $A$  is designated as  $L\{A\}^l$  after the Laplacian pyramid decomposition, and the  $l$ th layer of image  $B$  is designated as  $G\{B\}^l$  after the Gaussian pyramid decomposition. Then, when Eq. (18) is applied to each layer, the weighted sum is obtained using the weights in the weight map pyramid and the Laplacian pyramid coefficient of the corresponding position, which is the new Laplacian pyramid after fusion:

$$L\{R\}_{ij}^l = \sum_{k=1}^N G\{\hat{W}\}_{ij,k}^l \times L\{I\}_{ij,k}^l, \quad (18)$$

In Eq. (18),  $N$  is the number of input images;  $I$  is the number of input images with different exposure levels;  $ij$  is the pixel  $(i, j)$ ;  $\hat{W}$  is the weight after normalization; and  $l$  is the number of layers of the pyramid decomposition ( $0 \leq l \leq M$ ), with a default maximum number of 5.

Finally, the Laplacian pyramid  $LR^l$  is reconstructed to generate the fused image  $R$ . The fusion process is as follows:

$$R_{ij} = \sum_{l=0}^M L\{R\}_{ij}^l \uparrow^d, \quad (19)$$

In Eq. (19),  $\uparrow^d$  is the upsampling operator, and  $d$  is the sampling factor ( $d = 2^{l-1}$ ).

Fig. 8 shows the effect of the number of pyramid layers on the fusion effect. In which, (a) is original image; (b)–(e) fusion results obtained when the number of pyramid layers is set to 1, 3, 5, and 7, respectively. Clearly, the multiscale fusion method can effectively avoid the halo effect, and the increase in the number of layers can improve the overall visual effect of the image and highlight the scene details while enhancing the perception of reality.

### 3.4. Algorithm pipeline

The full processing pipeline of the proposed algorithm is as follows.<sup>1</sup>

---

#### Algorithm

---

**Input:** low-light image  $I$ , number of virtual exposure images  $N$ , levels of pyramid  $M$

**Output:** enhanced image  $J$

**Begin**

    (1) To generate virtual exposure images from input image

    1     for  $k = 1 : N$

    2          $I_k = \text{Virtual\_exposure}(I, f_k)$

    3     end

    (2) Calculate weight maps

    4     for  $k = 1 : N$

    5          $C_k = \text{Contrast}(I_k)$

    6          $S_k = \text{Saturation}(I_k)$

    7          $A_k = \text{Saliency}(I_k)$

    8          $W_k = C_k \times S_k \times A_k$

    9          $W_k = \text{Normalized}(W_k)$

    10    end

    (3) Pyramid decomposition

    11    for  $k = 1 : N$

    12          $W_{\text{pyr}} = \text{Gaussian\_pyramid}(W_k)$

    13          $I_{\text{pyr}} = \text{Laplacian\_pyramid}(I_k)$

    14         for  $l = 1 : M$

    15              $\text{Pyr}[l] = \text{Pyr}[l] + W_{\text{pyr}}[l] \times I_{\text{pyr}}[l]$

    16         end

    17    end

    (4) Reconstruct pyramid and output image

    18          $J = \text{Reconstruct\_laplacian\_pyramid}(\text{Pyr})$

**End**

---

### 4. Experimental results analysis

To test the effectiveness of the proposed algorithm, we built an experimental platform (computer processor: Intel (R) Core™ i7-6700 CPU @3.4 GHz; RAM: 16 GB) and designed experiments on five databases: the LDR dataset [48], the IEC dataset [49], the PMEA dataset [50], the LoL dataset [36] and a self-built dataset with 300 images. The common feature of those images is that each image has the regions of low brightness. Some typical experimental results are shown in Fig. 9, for each image, the dark region is from the low-light image, and the bright part is from the enhanced image. To better present the comparisons, each image was divided into two regions: one part is from the low-light

<sup>1</sup> <https://github.com/pumpkin8000/low-light-image-enhancement>

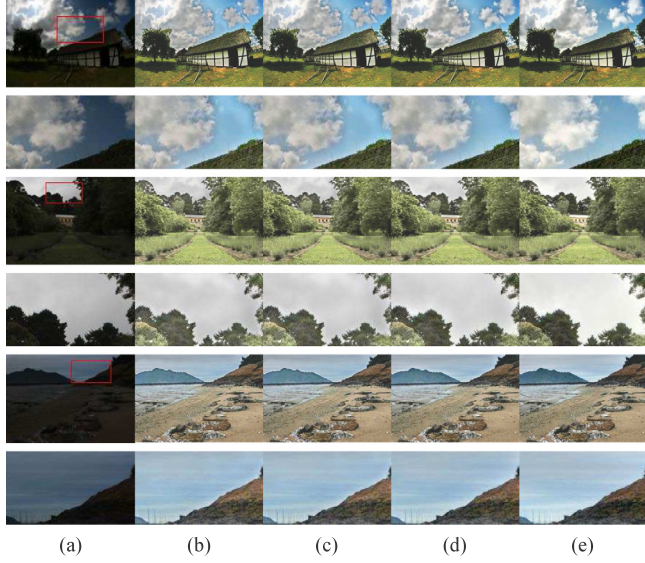


**Fig. 8.** Change in the image fusion effect with the number of pyramid layers. (a) original image; (b)–(e) fusion results when the number of pyramid layers is set to 1, 3, 5, and 7, respectively.



**Fig. 9.** Typical experimental results (for each image, the darker region is from the source image, and the brighter part is from the enhanced image).



**Fig. 10.** Edge detection results of images before and after enhancement. (a) is the original image; (b) is the edge detection on (a); (c) is the Enhanced image of (a); (d) is the edge detection on (c).

image, and the other part is from the enhanced image. Fig. 9 shows that after being processed with our algorithm, the dark regions of the low-light images were enhanced while avoiding overenhancement, which indicated that the proposed method performs well in low-light image enhancement.

To test the influence of image enhancement on feature extraction, we also designed edge detection and image matching experiments. Fig. 10 shows the edge detection result obtained using the Canny operator, in which Fig. 10(a) is the low-light image, Fig. 10(b) is the edge detection result obtained on the image in Fig. 10(a), Fig. 10(c) is the enhanced image, and Fig. 10(d) is the edge detection result obtained on the image in Fig. 10(c). The results show that the information under low light is visible and that the enhanced image has richer edges, which indicates that the proposed method can improve the image feature extraction performance.

Fig. 11 shows the result of image feature matching using the SIFT operator, in which images in the first and second rows are the low-light images and the enhanced images, respectively. Fig. 11(a) and (b)

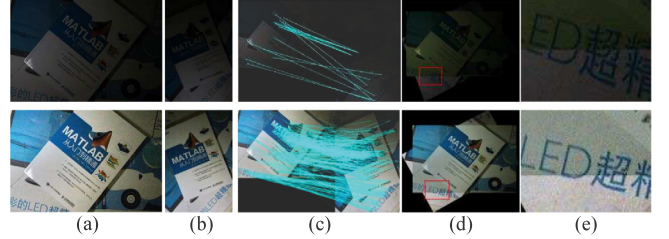


**Fig. 11.** Effect of image enhancement on image matching. (a) and (b) are two images to be matched, (c) shows the connections of the matching points, (d) is the matching result, and (e) is the enlargement of the area in the red rectangle shown in (d).

are two images to be matched, Fig. 11(c) shows the connections of the matching points, Fig. 11(d) is the matching result, and Fig. 11(e) is the enlargement of the area in the red rectangle shown in Fig. 11(d). Based on the processing data, 205 and 42 key points were detected in the two low-light images, respectively, from which 21 matching points were locked. Compared with the low-light images, 2425 and 2495 key points were found in the two enhanced images, from which 676 matching points were ultimately locked. The matching results in Fig. 11(d) and (e) show that the matching results of the two low-light images included mismatches, but accurate matching was achieved on the enhanced images using the same method. Therefore, the virtual multiple-exposure fusion algorithm proposed in this paper can improve both the visual effects and feature extraction.

Below, the proposed method is compared with various state-of-the-art algorithms developed in recent years, such as the camera response model (CRM) [51], the fractional-order fusion model (FFM) [52], the Gaussian total variation model (GTV) [1], the linking synaptic computation network (LSCN) [53], SRIE [20], KinD [41], MBLLEN [37], RetinexNet [36], and ZeroDCE [4], from the perspectives of subjective visual evaluation and objective quantitative analysis [54].

#### 4.1. Subjective evaluation

Figs. 12 and 13 show the results of a comparison between the proposed method and various mainstream methods. In which, (a) includes the low-light images, and (b)–(k) are the images enhanced using the CRM, KinD, MBLLEN, FFM, GTV, RetinexNet, LSCN, ZeroDCE, SRIE, and proposed methods, respectively. In Fig. 13, the enlarged regions indicated by the red rectangles are shown in rows 2, 4 and 6 on three images ('Rail', 'Girl', and 'Tower'). The results show that different degrees of improvement are achieved on the low-light images in terms of clarity and contrast after enhancement and that more details that are absent from the low-light image, revealing good enhancement effects.

Compared with other images, the enhanced images in (d), (h), and (j) show insufficient enhancement and noise amplification in dark regions, with much of the information remaining untapped. Particularly, for the 'Girl' and 'Tower' images, the MBLLEN and SRIE methods are unable to restore the color of low-light pixels, resulting in the under-enhancement shown in (d) and (j). The CRM, KinD, LSCN, RetinexNet and ZeroDCE methods enhance the overall brightness of the image, but the RetinexNet yields a hue shift, and the LSCN methods excessively enhance the gradient information of the image, leading to obvious overenhancement of the color or edges, while the CRM and ZeroDCE methods result in generally too bright images with inadequate contrast. In Figs. 12–13, (e) and (f) show that the FFM and GTV methods perform poorly in processing the light/dark-interlaced area, exhibiting an overall poorer effect than that of the proposed method, while the proposed method strikes a balance between contrast and brightness, generating a better enhancement effect. The comparison of local details of the frame region shows that the RetinexNet and LSCN methods give rise to noise in the edge area derived from overenhancement; the CRM and ZeroDCE methods result in poorer contrast; and the MBLLEN

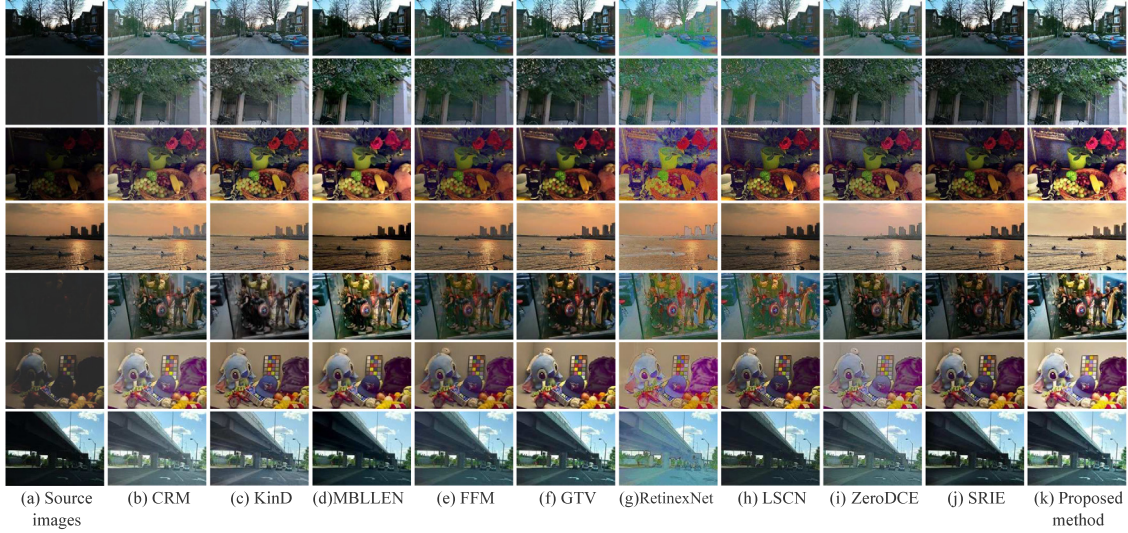


**Fig. 12.** Example of the experimental results. (a) includes the low-light images, and (b)–(k) are the images enhanced using the CRM, KinD, MBLLEN, FFM, GTV, RetinexNet, LSCN, ZeroDCE, SRIE, and proposed methods, respectively.

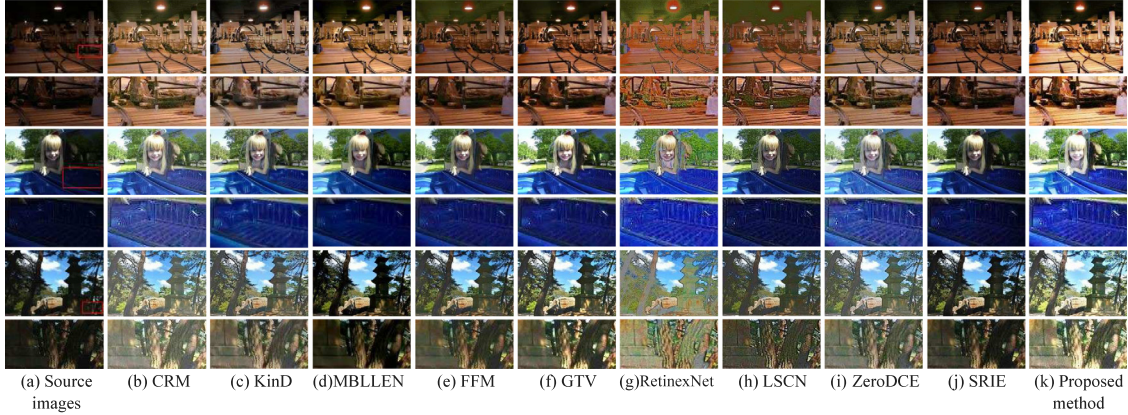


**Fig. 13.** Example of the experimental results with zoom-in regions. (a) includes the low-light images, and (b)–(k) are the images enhanced using the CRM, KinD, MBLLEN, FFM, GTV, RetinexNet, LSCN, ZeroDCE, SRIE, and proposed methods, respectively.

and SRIE methods cause various problems such as underenhancement and shadows in some local areas. In contrast, the proposed method shows a significant improvement in both color and contrast, achieving a significantly better visual result than the other methods, such as clear details and well-retained colors.

Fig. 14 shows the results of the enhancement effect relative to a reference image using the IEC database [49]. Fig. 14(a) and Fig. 14(b) are, respectively, the low-light image and reference image (normal-light image) of the same scene. The image pairs are named “Blanket.jpg”, “Building.jpg”, and “Car.jpg”. Fig. 14 (c)–(k) shows images enhanced with the CRM, KinD, FFM, GTV, RetinexNet, LSCN, ZeroDCE, SRIE and proposed methods, respectively. The results show that relative to the low-light images (Fig. 14(a)), the enhanced images obtained using the above nine algorithms restore the color to a large extent and markedly increase overall brightness as well as the information content of the images. Compared with the reference images (Fig. 14 (b)), the SRIE, GTV, and FFM methods perform poorly in presenting details; the LSCN method causes color distortion; the RetinexNet method causes overenhancement and loss of color information; and the CRM method performs similarly to the proposed method and have better contrast than the KinD and ZeroDCE methods, although the CRM method generally fails to present details. The images processed using the proposed method are similar to the reference images in terms of the overall color and contrast.

The above results show that the images enhanced by the proposed method show clearer image contours and a more natural overall effect than those obtained through other advanced methods, making it easier for viewers to see the key information displayed in each image. Therefore, from the perspective of a subjective evaluation, the proposed method well able to enhance low-light images.

#### 4.2. Objective analysis and evaluation

When evaluating image quality with the human eye, individuals may have different perceptions; thus, one-sidedness in the subjective evaluation result can easily occur. Therefore, in this section, objective quality evaluation indexes are introduced to assess the performance of the algorithms in terms of the objective data, and adequate data support is achieved regarding the image processing effectiveness [55].

##### (1) Evaluation of image quality without a reference

No-referenced indexes are usually used for evaluation [56–58]. In this paper, four no-reference evaluation indexes, i.e., entropy, CEIQ [59], JPEGC [60], and NIQE [61], were adopted as objective assessment metrics to measure the performances of the different methods. According to the theory of entropy, the higher the entropy value is, the greater the amount of information in an image and thus the richer the details. The CEIQ and JPEGC reflect the overall contrast of an image;



**Fig. 14.** Experimental comparisons with reference images. (a) includes the low-light images, (b) includes the reference images, (c)–(k) are the images enhanced using the CRM, KinD, FFM, GTV, RetinexNet, LSCN, ZeroDCE, SRIE, and proposed methods, respectively.

**Table 1**

Objective quality evaluation of images in Fig. 13.

	Metrics	CRM	KinD	MBLLEN	FFM	GTV	RetinexNet	LSCN	ZeroDCE	SRIE	Ours
Group 1	CEIQ	2.97	3.36	<u>3.45</u>	3.06	3.08	3.15	2.92	3.34	3.10	<b>3.48</b>
	JPEGC	29.27	<b>34.66</b>	33.54	19.48	14.06	30.44	25.30	25.07	19.79	<u>34.28</u>
	NIQE	2.90	3.84	3.71	3.31	<b>2.47</b>	6.39	4.80	2.86	<u>2.71</u>	3.21
	Entropy	7.20	7.25	<u>7.53</u>	6.82	6.92	6.91	6.84	7.25	6.97	<b>7.61</b>
Group 2	CEIQ	3.34	3.50	3.47	3.34	3.40	<u>3.53</u>	3.29	3.51	3.20	<b>3.66</b>
	JPEGC	33.11	39.18	33.12	34.34	30.81	<b>46.51</b>	47.88	39.27	33.00	<u>46.08</u>
	NIQE	2.89	<b>2.76</b>	2.87	2.99	3.16	4.13	5.05	3.16	<u>2.85</u>	3.31
	Entropy	7.58	7.65	<u>7.69</u>	7.43	7.52	7.62	7.46	7.64	7.35	<b>7.81</b>
Group 3	CEIQ	3.22	<u>3.42</u>	3.22	3.31	3.21	3.26	3.10	3.35	3.25	<b>3.58</b>
	JPEGC	37.83	41.86	43.06	36.45	32.66	<u>43.59</u>	39.39	40.00	37.51	<b>47.01</b>
	NIQE	<u>2.47</u>	2.73	3.11	2.65	<b>2.41</b>	5.43	4.73	3.23	2.76	2.95
	Entropy	7.42	7.44	<u>7.46</u>	7.36	7.21	7.27	7.18	7.40	7.32	<b>7.69</b>

(The best result is bolded and the second best one is underlined.)

the higher the CEIQ and JPEGC are, the higher the contrast and thus the richer the details. For the NIQE, a smaller value is better.

**Table 1** shows the objective evaluation results of the images in Fig. 13 enhanced using the CRM, KinD, MBLLEN, FFM, GTV, RetinexNet, LSCN, ZeroDCE, and SRIE method. It can be seen that our method can perform the best or second best values on the metrics of CEIQ, JPEGC and Entropy. However, like other deep-learning-based methods such as MBLLEN, RetinexNet, ZeroDCE, our method does not achieve satisfactory results on NIQE. This may be because there are too many artifacts in the image generated by fusion or deep learning, which affect the natural properties of the image itself.

To show the universality of the proposed method, the images from our self-built database, the LDR database, the IEC database, and the PMEA database were experimentally tested, in which the results of the same method on different images were averaged as the final result, using the following formula:

$$\bar{\lambda} = \sum_{i=1}^n \lambda_i, \quad (20)$$

where  $\lambda_i$  is the calculation result of the  $i$ th image and  $\bar{\lambda}$  is the average of the indicator values of all images in the database. **Table 2** shows a comparison of the proposed method with nine traditional methods on the four databases. The results show that the values of all three indexes (i.e., CEIQ, JPEGC, and entropy) of the proposed method are higher than those of the other methods when applied to the self-built database, the LDR database, and the PMEA database. On the IEC database, the proposed method outperforms the other methods in terms of the entropy and CEIQ. To the metric of NIQE, as discussed on **Table 1**, our method, KinD, MBLLEN, RetinexNet, ZeroDCE, achieved no best results, while FFM and GTV shows the excellent performance on this index.

Over all, the results show that among the twelve groups of data, the proposed method outperforms the other methods on eight groups of data, indicating that the proposed method performs better overall than the other methods.

#### (2) Image quality assessment with reference images

The image pair (low-light image and its reference image) shown in Fig. 14 was evaluated and compared in terms of the peak signal-to-noise

ratio (PSNR), structural similarity index (SSIM) [62,63], visual information fidelity (VIF) [64], and information fidelity criterion (IFC) [65]. The PSNR reflects the difference in the image before and after processing. The higher the PSNR value is, the smaller the difference. The SSIM reflects the correlation between adjacent pixels, conveys the structural information of the objects in a scene, and measures the structural distortion of an image. The higher the SSIM value is, the higher the structural similarity between two pixels. The evaluation results of the images in Fig. 14 are shown in **Table 3**. The results show that for the four evaluation indicators, the proposed method has the highest values on images ‘Blanket’ and ‘Building’. For image ‘Car’, the values of the PSNR and IFC of the proposed method are lower than those of the KinD method and the ZeroDCE method, respectively, but the values of the other two indexes of the proposed method are higher than those of all other methods, which demonstrates the outstanding performance of the proposed algorithm.

To verify the generality of the results, the IEC database [49] and LoL database [36] were used in the experiment. The results in **Table 4** show that in terms of the VIF and IFC, the proposed method is superior to all the other methods, while in terms of the SSIM and PSNR, it is inferior to the KinD and FFM methods. Out of all eight indicators, our method, KinD and FFM achieve the best values for four, three and one of them, respectively. The above results indicate that the proposed method can enhance the brightness of an image while avoiding the distortion of information, such as color and structure, thereby maintaining a high similarity with the images acquired under fine lighting conditions.

All the above results calculated on various databases indicate that in terms of objective quality assessment metrics, the images enhanced using the proposed method are superior to those enhanced using other methods, which is consistent with the conclusion of the subjective evaluation. Overall, our results verify that it is effective and feasible to use the abovementioned indicators to evaluate the quality of enhanced images.

#### 4.3. Adaptive analysis

The enhancement of images acquired under extremely poor lighting conditions has long been challenging, as conventional methods are

**Table 2**

Objective quality evaluation on images from Self-built database, LDR database, IEC database, and PMEA database, enhanced with different methods.

	Metrics	CRM	KinD	MBLLEN	FFM	GTV	RetinexNet	LSCN	ZeroDCE	SRIE	Ours
Self-built database	CEIQ	3.16	3.23	<u>3.31</u>	3.14	3.08	3.13	3.04	3.21	3.13	<b>3.38</b>
	JPEGC	25.45	<u>30.04</u>	29.33	22.16	15.90	29.26	24.31	24.85	22.96	<b>32.71</b>
	NIQE	3.36	3.41	3.63	<u>3.23</u>	<b>3.21</b>	4.42	4.56	3.51	3.30	3.41
	Entropy	7.23	7.16	<u>7.33</u>	7.02	6.97	6.98	6.91	7.13	7.08	<b>7.44</b>
LDR database	CEIQ	3.18	3.20	<b>3.33</b>	3.20	3.12	3.17	3.03	3.21	3.15	<b>3.29</b>
	JPEGC	23.26	<b>32.45</b>	26.61	21.98	<b>15.14</b>	29.82	22.92	23.93	21.33	<b>31.37</b>
	NIQE	<u>3.07</u>	3.36	3.46	<b>2.93</b>	3.11	4.37	4.33	3.41	3.22	3.43
	Entropy	7.29	7.09	<b>7.37</b>	7.12	7.04	7.07	6.88	7.18	7.11	7.35
IEC database	CEIQ	3.21	3.09	<u>3.32</u>	2.88	2.87	2.77	3.09	2.93	3.00	<b>3.35</b>
	JPEGC	23.07	<u>25.51</u>	<b>30.70</b>	12.88	7.38	15.40	16.49	13.98	14.59	22.98
	NIQE	3.75	3.91	4.44	<b>3.65</b>	3.80	4.94	6.05	3.96	<u>3.67</u>	3.88
	Entropy	<u>7.33</u>	6.92	7.27	6.57	6.62	6.53	6.97	6.67	6.83	<b>7.36</b>
PMEA database	CEIQ	3.09	3.31	<u>3.33</u>	3.11	3.09	3.15	2.91	3.28	3.15	<b>3.51</b>
	JPEGC	26.25	<u>30.84</u>	31.18	22.12	15.94	28.86	20.88	25.99	24.04	<b>35.49</b>
	NIQE	3.21	3.42	3.71	<u>3.18</u>	<b>3.01</b>	4.46	4.29	3.44	<u>3.18</u>	<b>3.18</b>
	Entropy	7.19	7.32	<u>7.42</u>	7.01	7.00	7.03	6.78	7.24	7.13	<b>7.62</b>

(The best result is bolded and the second best one is underlined.)

**Table 3**

Objective quality evaluation on images in Fig. 14 enhanced using different methods.

	Metrics	CRM	KinD	FFM	GTV	RetinexNet	LSCN	ZeroDCE	SRIE	Ours
Group 1	SSIM	0.54	0.90	0.84	0.68	0.71	0.75	<u>0.91</u>	0.82	<b>0.93</b>
	VIF	0.30	0.51	0.42	0.43	0.42	0.37	<u>0.57</u>	0.50	<b>0.58</b>
	IFC	2.60	3.95	3.57	4.06	3.06	2.69	<b>4.59</b>	4.09	<b>4.41</b>
	PSNR	15.38	<b>23.59</b>	17.17	13.70	16.93	18.76	20.67	15.23	23.40
Group 2	SSIM	0.69	0.89	0.87	0.79	0.77	0.82	<b>0.92</b>	0.79	<b>0.92</b>
	VIF	0.44	0.47	0.46	0.46	0.39	0.38	<u>0.54</u>	0.48	<b>0.60</b>
	IFC	2.24	2.31	2.34	2.52	1.72	1.72	<u>2.61</u>	2.48	<b>2.81</b>
	PSNR	14.93	15.69	12.90	13.05	13.91	15.21	<u>17.51</u>	12.83	<b>20.09</b>
Group 3	SSIM	0.44	0.73	<u>0.76</u>	0.64	0.56	0.68	0.73	0.66	<b>0.84</b>
	VIF	0.25	0.35	0.31	0.31	0.26	0.27	<u>0.36</u>	0.33	<b>0.39</b>
	IFC	2.46	3.23	3.01	3.19	2.33	2.40	<u>3.35</u>	3.20	<b>3.58</b>
	PSNR	10.92	<u>16.57</u>	13.86	11.89	15.28	15.67	16.13	12.09	<b>20.37</b>

(The best result is bolded and the second best one is underlined.)

**Table 4**

Objective quality evaluation on images from IEC database, LoL database, enhanced using different methods.

	Metrics	CRM	KinD	FFM	GTV	RetinexNet	LSCN	ZeroDCE	SRIE	Ours
IEC database	SSIM	0.64	0.82	<b>0.87</b>	0.81	0.66	0.73	0.83	<u>0.85</u>	0.84
	VIF	0.41	0.45	0.42	0.41	0.37	0.42	0.47	<u>0.48</u>	<b>0.55</b>
	IFC	2.49	2.72	2.75	2.87	2.08	2.29	2.89	<u>3.00</u>	<b>3.16</b>
	PSNR	15.62	<b>18.73</b>	17.66	16.68	14.73	17.87	<u>18.58</u>	17.30	18.13
LoL database	SSIM	0.38	<b>0.87</b>	0.72	0.51	0.70	0.58	0.71	0.59	0.73
	VIF	0.28	<u>0.43</u>	0.36	0.33	0.31	0.31	0.40	0.39	<b>0.44</b>
	IFC	1.38	<u>2.06</u>	2.02	2.00	1.42	1.39	1.98	2.02	<b>2.07</b>
	PSNR	11.72	<b>19.71</b>	13.34	10.54	17.03	15.79	14.57	11.56	<u>17.13</u>

(The best result is bolded and the second best one is underlined.)

prone to cause overenhancement, halo effects, or color distortion. To verify the robustness of the proposed method, it was tested on several challenging images acquired under extremely low lighting, at nighttime, and with backlighting. The experimental results are shown in Fig. 15, in which the first and second columns of Fig. 15(a), (b), and (c) present the low-light images and their corresponding enhanced images, respectively. The results show that the proposed method exhibits a satisfactory enhancement effect that increases the brightness of dark areas while avoiding noise amplification, giving rise to better clarity, contrast, and color and thereby being consistent with human visual perception. Especially for the nighttime scenes with uneven lighting, such as point lighting and backlighting, the proposed method does not cause marked overenhancement in the well-lit regions when increasing the brightness of the poorly lit regions, indicating that the proposed method can adaptively adjust parameters for different scenarios, ensuring high robustness and adaptability. The proposed method was also compared with several pieces of commercial application software that have the function of ‘one-click enhancement’, including the online

tools such as Tuyitu<sup>2</sup> Meitu,<sup>3</sup> and Baidu.<sup>4</sup> The testing images captured under various poor lighting conditions, such as nighttime, overcast, uneven lighting, and backlighting. The representative results are shown in Fig. 16. Enhancement of the images using our method significantly improves the brightness and reveals the detailed information of images taken under poor lighting. In contrast, the enhancement using the other methods is poor. These results indicate that the adaptive enhancement of the proposed method has outstanding advantages that allow the presentation of details without overenhancement and with high robustness.

#### 4.4. Comparison of different exposure functions

As discussed in Section 3.1, to the virtual exposure enhancer, we can also generate the sub-images with other nonlinear functions on the

<sup>2</sup> <https://www.tuyitu.com/photoeditor/>

<sup>3</sup> <https://xiuxiu.web.meitu.com/main.html>

<sup>4</sup> <https://ai.baidu.com/>

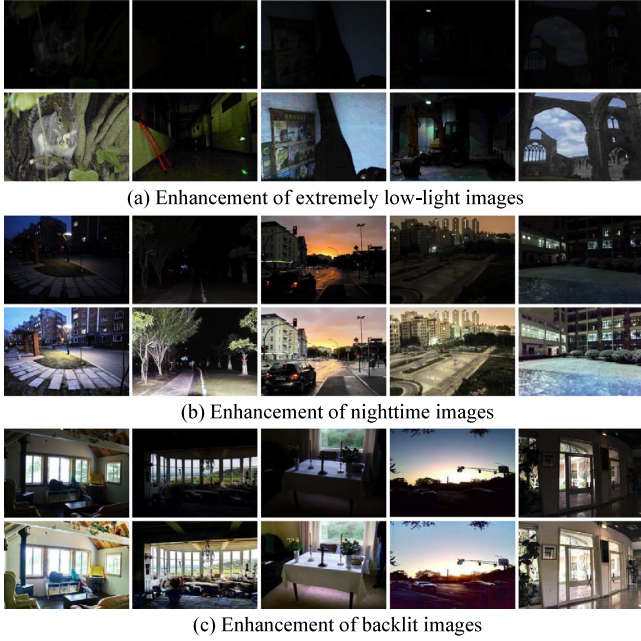


**Fig. 15.** Examples of image enhancement under different lighting conditions. (a), (b), and (c) present the low-light images and their corresponding enhanced images, respectively.



**Fig. 16.** Comparison of the proposed method with commercial software. (The testing images captured under various poor lighting conditions, such as nighttime, overcast, uneven lighting, and backlighting are compared with Meitu, Tuyitu, Baidu and our method.)

input image. The experimental results with gamma function ( $\gamma$  is setting to 0.2, 0.3, 0.4, 0.5, 0.6, 1, respectively) and our quadratic function are shown in Fig. 17.

It can be seen that, comparing with gamma function method, the enhanced result of quadratic function method has higher brightness, stronger contrast and more realistic. Which mainly because our method can simulate the process of strong exposure while the value of gamma function cannot break through the limit of the output value of 1.

#### 4.5. Failure cases

Although the proposed method can enhance the dark regions in a low-light image, it has obvious weaknesses that it does not have the ability to suppress the brightness of overexposed areas. Some failure

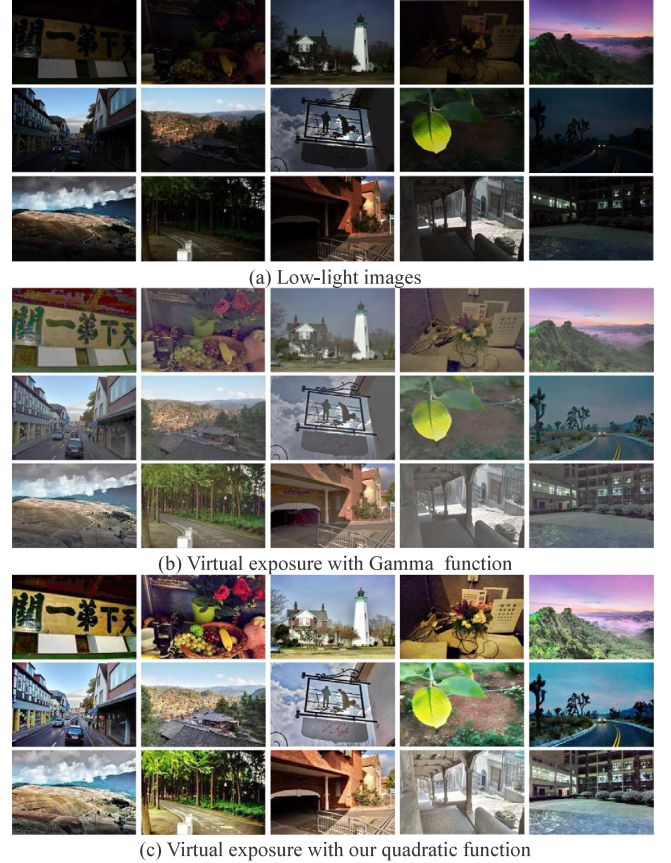


**Fig. 17.** Comparison of different exposure functions.

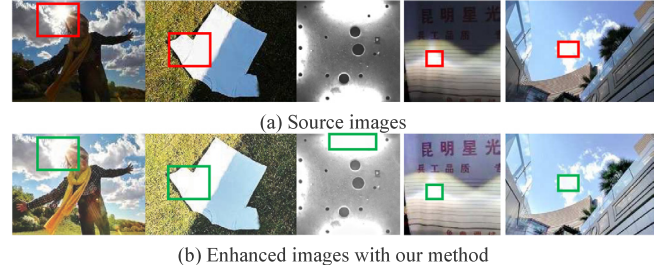


**Fig. 18.** Failure cases of enhancement for the images containing over-exposure areas (the overenhanced regions are marked with color rectangles).

cases are shown in Fig. 18, in which the overenhanced regions are marked with color rectangles. It can be seen that the dark areas are enhanced while the brightness of the overexposed areas are almost unchanged. The reason of this question is that the key idea of this method is to mine the information of the enhanced low brightness area through information fusion, which lacks the mechanism to deal with the over exposed area. From Eqs. (6) and (7), it also could be proved that the virtual exposure enhancer could not deal with the overexposed areas.

## 5. Conclusions

In this paper, an adaptive single-image enhancement framework that combines a virtual exposure strategy with image fusion is proposed, aiming at addressing the problem of local under/overenhancement and the lack of adaptability of parameter setting in traditional methods. This method is different from the traditional

multiexposure image fusion in that only a single image is used for generating multiexposure images with a virtual intensifier, after which an image sequence with different details can be fused to generate a clear image. Compared with the state-of-the-art enhancement methods on five datasets, the results show that the output of our method has less brightness distortion and color distortion and can effectively retain the visual information of the image itself, which is more in line with the visual perception of the human eyes. More importantly, this method does not require camera response curve calibration and tracking the exposure time of each photo. The parameters that need to be transformed are automatically calculated and obtained. It is self-adaptively and robustness, and can be applied to video monitoring, scene recovery and other fields. However, because this algorithm could not deal with the overexposed areas, how to improve the algorithm's performance of suppressing the brightness of overexposed areas will be the next research focus in the future.

#### CRediT authorship contribution statement

**Wencheng Wang:** Conception or design of the work, Acquisition, Analysis or interpretation of data for the work. **Dongliang Yan:** Code programing and test. **Xiaojin Wu:** Polished the paper, Designed the optimization scheme. **Weikai He:** Done the references collection. **Zhenxue Chen:** Drafted the work or revised it critically for important intellectual content. **Xiaohui Yuan:** Polished the paper including language, grammar. **Lun Li:** Made the software drawing.

#### Declaration of competing interest

The authors declare that they have no known competing financial interests or personal relationships that could have appeared to influence the work reported in this paper.

#### Data availability

Data will be made available on request.

#### References

- [1] S. Hao, X. Han, Y. Guo, X. Xu, M. Wang, Low-light image enhancement with semi-decoupled decomposition, *IEEE Trans. Multimed.* 22 (12) (2020) 3025–3038.
- [2] Q. Wang, W. Chen, X. Wu, Z. Li, Detail-enhanced multi-scale exposure fusion in YUV color space, *IEEE Trans. Circuits Syst. Video Technol.* 30 (8) (2020) 2418–2429.
- [3] W. Wang, Z. Chen, X. Yuan, X. Wu, Adaptive image enhancement method for correcting low-illumination images, *Inform. Sci.* 496 (2019) 25–41.
- [4] C. Guo, C. Li, J. Guo, C. Loy, J. Hou, S. Kwong, R. Cong, Zero-reference deep curve estimation for low-light image enhancement, in: *IEEE Conference on Computer Vision and Pattern Recognition*, 2020, pp. 1780–1789.
- [5] W. Wang, Z. Chen, X. Yuan, Simple low-light image enhancement based on Weber-Fechner law in logarithmic space, *Signal Process., Image Commun.* (2022) 116742.
- [6] S. Boyina, Dynamic histogram equalization for contrast enhancement for digital images, *Appl. Soft Comput.* 89 (2020) 106114.
- [7] T. Kim, J. Paik, B. Kang, Contrast enhancement system using spatially adaptive histogram equalization with temporal filtering, *IEEE Trans. Consum. Electron.* 44 (1) (1998) 82–87.
- [8] A.M. Reza, Realization of the contrast limited adaptive histogram equalization (CLAHE) for real-time image enhancement, *J. VLSI Signal Process. Syst. Signal Image Video Technol.* 38 (1) (2004) 35–44.
- [9] G. Campos, S. Mastelini, G. Aguiar, R. Mantovani, S. Barbon, Machine learning hyperparameter selection for contrast limited adaptive histogram equalization, *EURASIP J. Image Video Process.* (2019) 59.
- [10] T. Celik, T. Tjahjadi, Contextual and variational contrast enhancement, *IEEE Trans. Image Process.* 20 (12) (2011) 3431–3441.
- [11] A. Parihar, O. Verma, Contrast enhancement using entropy-based dynamic sub-histogram equalisation, *IET Image Process.* 10 (11) (2016) 799–808.
- [12] K. Gu, G. Zhai, W. Lin, M. Liu, The analysis of image contrast: From quality assessment to automatic enhancement, *IEEE Trans. Cybern.* 46 (1) (2017) 284–297.
- [13] Y. Liu, J. Guo, J. Yu, Contrast enhancement using stratified parametric-oriented histogram equalization, *IEEE Trans. Circuits Syst. Video Technol.* 27 (6) (2017) 1171–1181.
- [14] M. Zarie, A. Pourmohammad, H. Hajghassem, Image contrast enhancement using triple clipped dynamic histogram equalization based on standard deviation, *IET Image Process.* 13 (7) (2019) 1081–1089.
- [15] Z. Rahman, D. Jobson, G. Woodell, Retinex processing for automatic image enhancement, *J. Electron. Imaging* 13 (1) (2004) 100–110.
- [16] W. Wang, X. Wu, X. Yuan, Z. Gao, An experiment-based review of low-light image enhancement methods, *IEEE Access* 8 (1) (2020) 87884–87917.
- [17] A. Petro, C. Sbert, J. Morel, Multiscale Retinex, *Image Process. Line* (4) (2014) 71–88.
- [18] M. Li, J. Liu, W. Yang, X. Sun, Z. Guo, Structure-revealing low-light image enhancement via robust Retinex model, *IEEE Trans. Image Process.* 27 (6) (2018) 2828–2841.
- [19] S. Wang, J. Zheng, H. Hu, B. Li, Naturalness preserved enhancement algorithm for non-uniform illumination images, *IEEE Trans. Image Process.* 22 (9) (2013) 3538–3548.
- [20] X. Fu, D. Zeng, Y. Huang, X. Zhang, X. Ding, A weighted variational model for simultaneous reflectance and illumination estimation, in: *IEEE Conference on Computer Vision and Pattern Recognition*, 2016, pp. 2782–2790.
- [21] Y. Zhang, W. Huang, W. Bi, G. Gao, Colorful image enhancement algorithm based on guided filter and Retinex, in: *IEEE International Conference on Signal and Image Processing*, 2017, pp. 33–36.
- [22] W. Ji, Z. Qian, B. Xu, D. Zhao, A nighttime image enhancement method based on Retinex and guided filter for object recognition of apple harvesting robot, *Int. J. Adv. Robot. Syst.* 15 (1) (2018) 112–122.
- [23] M. Li, J. Liu, W. Yang, X. Sun, Z. Guo, Structure-revealing low-light image enhancement via robust Retinex model, *IEEE Trans. Image Process.* 27 (6) (2018) 2828–2841.
- [24] Z. Gu, F. Li, F. Fang, G. Zhang, A novel Retinex-based fractional-order variational model for images with severely low light, *IEEE Trans. Image Process.* 29 (2020) 3239–3253.
- [25] X. Ren, W. Yang, W. Cheng, J. Liu, LR3M: Robust low-light enhancement via low-rank regularized Retinex model, *IEEE Trans. Image Process.* 29 (2020) 5862–5876.
- [26] X. Dong, G. Wang, Y. Pang, W. Li, Y. Lu, Fast efficient algorithm for enhancement of low lighting video, in: *IEEE International Conference on Multimedia and Expo*, Washington, 2011, pp. 1–6.
- [27] C. Yu, X. Xu, H. Lin, X. Ye, Low-illumination image enhancement method based on a fog-degraded model, *J. Image Graphics* 22 (9) (2017) 1194–1205, (in Chinese).
- [28] L. Zhang, P. Shen, X. Peng, G. Zhu, J. Song, W. Wei, Simultaneous enhancement and noise reduction of a single low-light image, *IET Image Process.* 10 (11) (2017) 840–847.
- [29] Y. Hu, Y. Shang, X. Fu, H. Ding, Low-illumination video enhancement algorithm based on combined atmospheric physical model and luminance transmission map, *J. Image Graphics* 21 (8) (2016) 1010–1020, (in Chinese).
- [30] S. Park, B. Moon, S. Ko, S. Yu, J. Paik, Low-light image restoration using bright channel prior-based variational Retinex model, *EURASIP J. Image Video Process.* 44 (2017) 1–11.
- [31] L. Tao, C. Zhu, J. Song, T. Lu, X. Xie, Low-light image enhancement using CNN and bright channel prior, in: *IEEE International Conference on Image Processing*, 2018, pp. 3215–3219.
- [32] H. Lee, K. Sohn, D. Min, Unsupervised low-light image enhancement using bright channel prior, *IEEE Signal Process. Lett.* 27 (2020) 251–255.
- [33] K.G. Lore, A. Akintayo, S. Sarkar, LLNet: A deep autoencoder approach to natural low-light image enhancement, *Pattern Recognit.* 61 (2016) 650–662.
- [34] L. Shen, Z. Yue, F. Feng, Q. Chen, S. Liu, J. Ma, MSR-net: low-light image enhancement using deep convolutional network, 2017, arXiv:1711.02488v1.
- [35] L. Tao, C. Zhu, G. Xiang, Y. Li, H. Jia, X. Xie, LLCNN: A convolutional neural network for low-light image enhancement, in: *IEEE Conference on Visual Communications and Image Processing*, 2018, pp. 1–4.
- [36] C. Wei, W. Wang, W. Yang, J. Liu, Deep retinex decomposition for low-light enhancement, in: *The British Machine Vision Conference*, 2018.
- [37] F. Lv, F. Lu, J. Wu, C. Lim, MBLLEN: Low-light image/video enhancement using CNNs, in: *The British Machine Vision Conference*, 2018, pp. 1–13.
- [38] M. Gharbi, J. Chen, J. Barron, S. Hasinoff, F. Durand, Deep bilateral learning for real-time image enhancement, *ACM Trans. Graph.* 36 (4) (2017) 118.
- [39] W. Wang, C. Wei, W. Yang, J. Liu, GLADNet: Low-light enhancement network with global awareness, in: *IEEE International Conference on Automatic Face & Gesture Recognition*, 2018, pp. 751–755.
- [40] C. Li, J. Guo, F. Porikli, Y. Pang, LightenNet: A convolutional neural network for weakly illuminated image enhancement, *Pattern Recognit. Lett.* 104 (2018) 15–22.
- [41] Y. Zhang, J. Zhang, X. Guo, Kindling the darkness: A practical low-light image enhancer, 2019, arXiv:1905.04161.

- [42] Y. Meng, D. Kong, Z. Zhu, Y. Zhao, From night to day: GANs based low quality image enhancement, *Neural Process. Lett.* 50 (1) (2019) 799–814.
- [43] S. Liu, Y. Zhang, Detail-preserving underexposed image enhancement via optimal weighted multi-exposure fusion, *IEEE Trans. Consum. Electron.* 65 (3) (2019) 303–311.
- [44] M. Zhu, P. Pan, W. Chen, Y. Yang, EEMEFN: Low-light image enhancement via edge-enhanced multi-exposure fusion network, in: Proceedings of the AAAI Conference on Artificial Intelligence, 2020, pp. 13106–13113.
- [45] X. Fu, D. Zeng, H. Yue, Y. Liao, X. Ding, J. Paisley, A fusion-based enhancing method for weakly illuminated images, *Signal Process.* 129 (2016) 82–96.
- [46] C. Ancuti, C.O. Ancuti, T. Haber, P. Bekaert, Enhancing underwater images and videos by fusion, in: IEEE Conference on Computer Vision and Pattern Recognition, 2012, pp. 81–88.
- [47] K. Gu, G. Zhai, X. Yang, W. Zhang, C.W. Chen, Automatic contrast enhancement technology with saliency preservation, *IEEE Trans. Circuits Syst. Video Technol.* 25 (9) (2015) 1480–1494.
- [48] C. Lee, C. Lee, C. Kim, Contrast enhancement based on layered difference representation of 2D histograms, *IEEE Trans. Image Process.* 22 (12) (2013) 5372–5384.
- [49] S. Cristiano, L. Paulo, S. Silvia, Deep learning based exposure correction for image exposure correction with application in computer vision for robotics, in: 2018 Latin American Robotic Symposium, 2018.
- [50] P. Tian, W. Shuhang, Perceptually motivated enhancement method for non-uniformly illuminated images, *IET Comput. Vis.* 12 (4) (2018) 424–433.
- [51] Z. Ying, G. Li, Y. Ren, R. Wang, W. Wang, A new low-light image enhancement algorithm using camera response model, in: IEEE International Conference on Computer Vision, 2017, pp. 3015–3022.
- [52] Q. Dai, Y. Pu, Z. Rahman, M. Aamir, Fractional-order fusion model for low-light image enhancement, *Symmetry* 11 (2019) 1–17.
- [53] K. Zhan, J. Shi, J. Teng, Q. Li, M. Wang, F. Lu, Linking synaptic computation for image enhancement, *Neurocomputing* 238 (7) (2017) 1–12.
- [54] K. Gu, X. Xu, J. Qiao, Q. Jiang, W. Lin, D. Thalmann, Learning a unified blind image quality metric via on-line and off-line big training instances, *IEEE Trans. Big Data* 6 (4) (2019) 780–791.
- [55] K. Gu, J. Qiao, S. Lee, H. Liu, W. Lin, P. Callet, Multiscale natural scene statistical analysis for no-reference quality evaluation of DIBR-synthesized views, *IEEE Trans. Broadcast.* 66 (1) (2020) 127–139.
- [56] G. Zhai, W. Sun, X. Min, J. Zhou, Perceptual quality assessment of low-light image enhancement, *ACM Trans. Multimed. Comput. Commun. Appl.* 17 (4) (2021) 1–24.
- [57] K. Gu, G. Zhai, X. Yang, W. Zhang, Hybrid no-reference quality metric for singly and multiply distorted images, *IEEE Trans. Broadcast.* 60 (3) (2014) 555–567.
- [58] Z. Zhang, W. Sun, X. Min, W. Zhu, T. Wang, W. Liu, G. Zhai, A no-reference evaluation metric for low-light image enhancement, in: IEEE International Conference on Multimedia and Expo, ICME, 2021, pp. 1–6.
- [59] J. Yan, J. Li, X. Fu, No-reference quality assessment of contrast-distorted images using contrast enhancement, 2019, arXiv:1904.08879.
- [60] Z. Wang, H. Sheikh, A. Bovik, No-reference perceptual quality assessment of JPEG compressed images, in: IEEE International Conference on Image Processing, 2002, pp. 477–480.
- [61] A. Mittal, R. Soundararajan, A. Bovik, Making a completely blind image quality analyzer, *IEEE Signal Process. Lett.* 20 (3) (2013) 209–212.
- [62] W. Zhou, A.C. Bovik, H.R. Sheikh, E. Simoncelli, Image quality assessment: From error visibility to structural similarity, *IEEE Trans. Image Process.* 13 (4) (2004) 600–612.
- [63] W. Wang, X. Yuan, X. Wu, Y. Liu, Fast image dehazing method based on linear transformation, *IEEE Trans. Multimed.* 19 (6) 1142–1155.
- [64] H. Sheikh, A. Bovik, Image information and visual quality, *IEEE Trans. Image Process.* 15 (2) (2006) 430–444.
- [65] H. Sheikh, A. Bovik, G. Veciana, An information fidelity criterion for image quality assessment using natural scene statistics, *IEEE Trans. Image Process.* 14 (12) (2006) 2117–2128.